Обзор ArXiv/astro-ph, 16-20 ноября 2020

От Сильченко О.К.

ArXiv: 2011.09924

Searching for intergalactic star forming regions in Stephan's Quintet with SITELLE: II. Physical properties and metallicity

S. Duarte Puertas[1], J. M. Vilchez[1], J. Iglesias-Páramo[1], L. Drissen[2,3], C. Kehrig[1], T. Martin[2,3], E. Pérez-Montero[1], and A. Arroyo-Polonio[1]

[1] Instituto de Astrofísica de Andalucía - CSIC, Glorieta de la Astronomía s.n., 18008 Granada, Spain
e-mail: salvini@iaa.es
[2] Département de physique, de génie physique et d'optique, Université Laval, Québec (QC), G1V 0A6, Canada
[3] Centre de recherche en astrophysique du Québec

Received November 20, 2020; accepted November 20, 2020

ABSTRACT

Based on SITELLE spectroscopy data, we studied the ionised gas emission for the 175 Hα emission regions in the Stephan's Quintet (SQ). In this paper we perform a detailed analysis of the star formation rate (SFR), oxygen abundance, and nitrogen-to-oxygen abundance ratio (N/O) of the SQ regions, with the intention of exploring the provenance and evolution of this complex structure. According to the BPT diagram, we found 91 HII, 17 composite, and 7 active galactic nucleus-like regions in SQ. Several regions are compatible with fast shocks models without a precursor for solar metallicity and low density (n = 0.1 cm^{-3}), with velocities in the range of 175 – 300 km s^{-1}. We derived the total SFR in SQ (log(SFR/M$_\odot$ yr^{-1}=0.496). Twenty-eight percent of the total SFR in SQ comes from starburst A, while 9% is in starburst B, and 45% comes from the regions with a radial velocity lower than 6160 km s^{-1}. For this reason, we assume that the material prior to the collision with the new intruder does not show a high SFR, and therefore SQ was apparently quenched. When considering the integrated SFR for the whole SQ and the new intruder, we found that both zones have a SFR consistent with those obtained in the SDSS star-forming galaxies. At least two chemically different gas components cohabit in SQ where, on average, the regions with high radial velocities (v>6160 km s^{-1}) have lower values of oxygen abundance and N/O than

SITELLE/CFHT

- Фурье-спектрометр на основе интерферометра Майкельсона
- Изначально предполагалось переменное спектральное разрешение, теперь вроде остановились на R=10000
- Поле 11’x11’, пиксель 0.32’’
- Три рабочих спектральных диапазона: УФ ([OII]3727), зеленый ([OIII], H-beta) и красный (H-alpha, [NII], [SII]).

Профили линий – свертка гауссианы и sinc

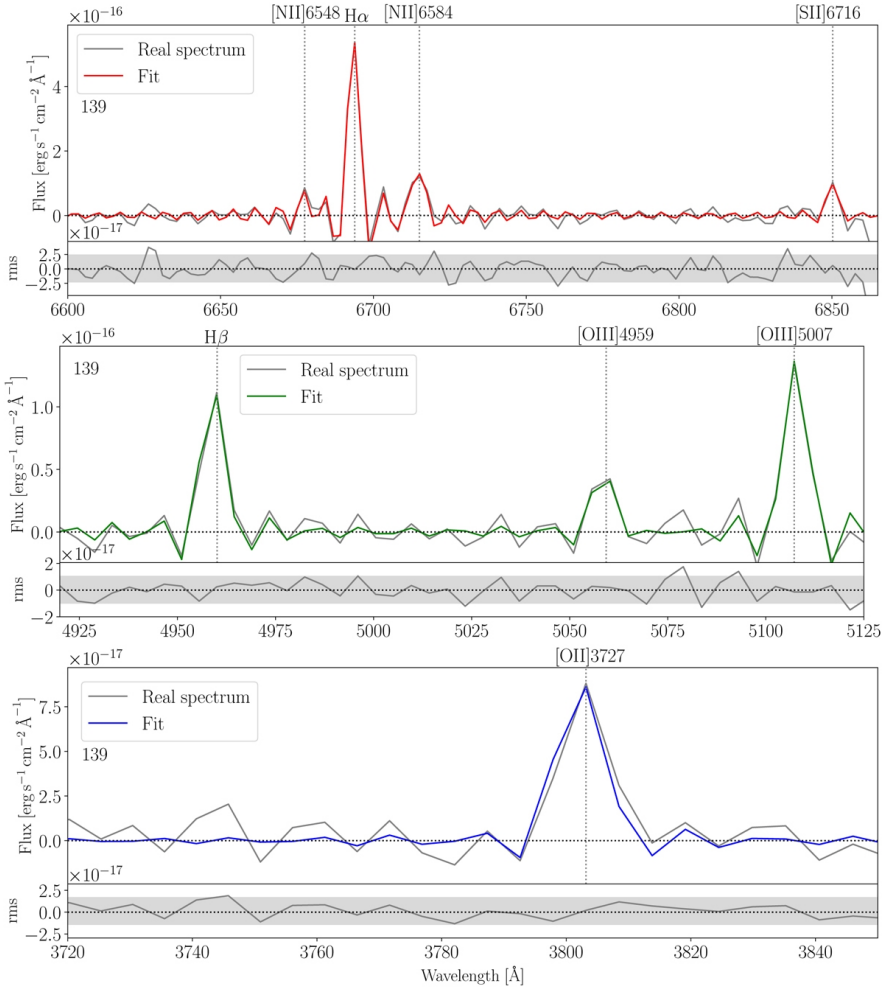

Квинтет Стефана

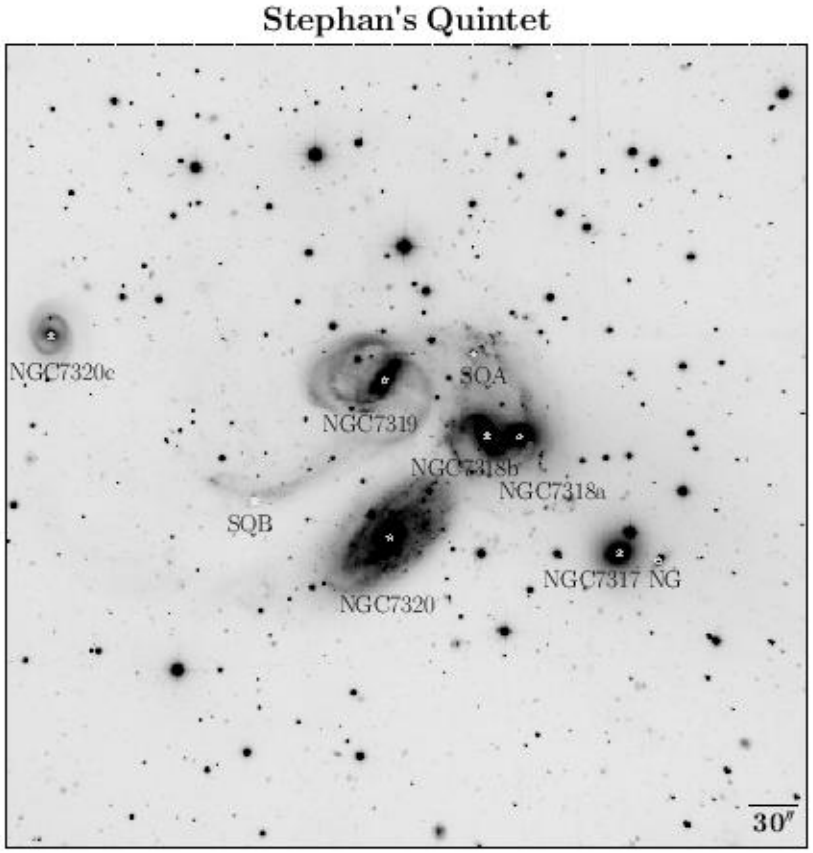

Fig. 1. SITELLE deep-greyscale image of SQ composed using SN1, SN2, and SN3 data cubes. North is top and East is left. The distance considered for SQ in this paper is d = 88.6 Mpc (from the NASA/IPAC Extragalactic Database known as NED). At the distance of SQ, 30″ corresponds to ~13.04 kpc.

Много газа и звездообразования МЕЖДУ галактиками

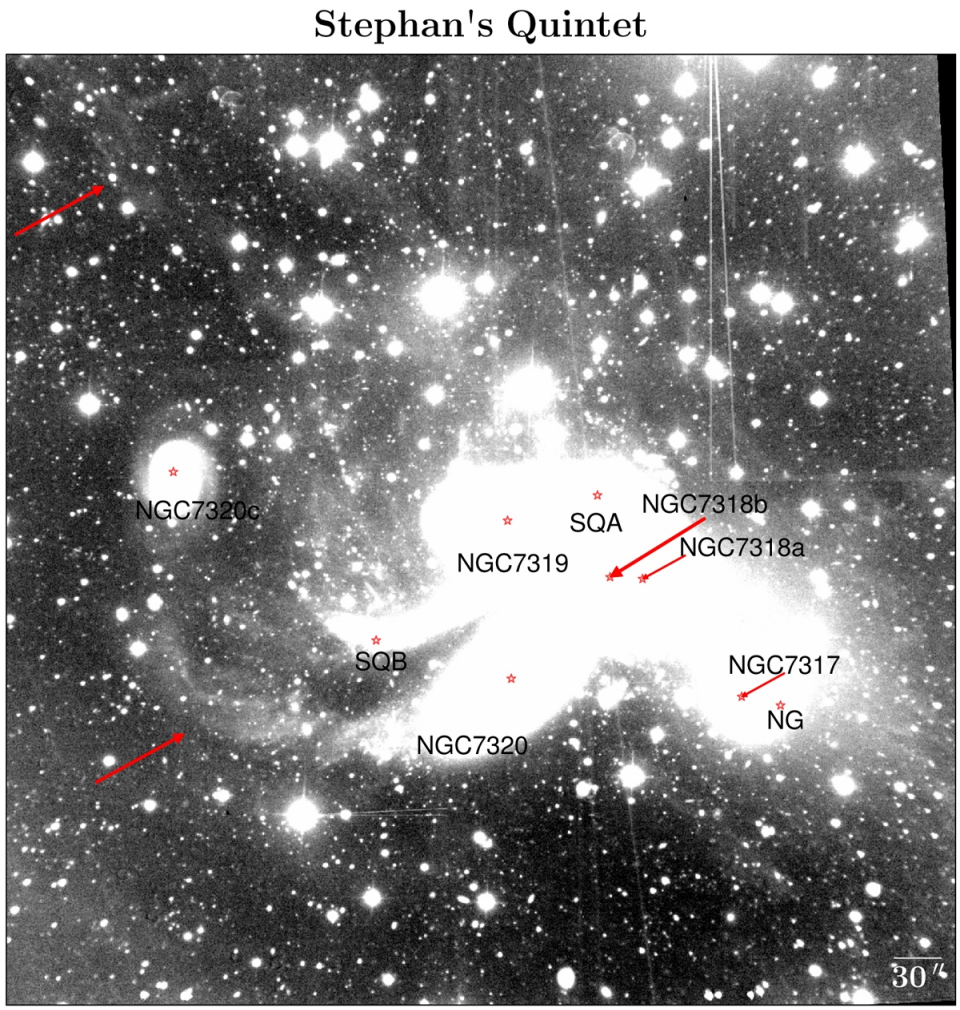

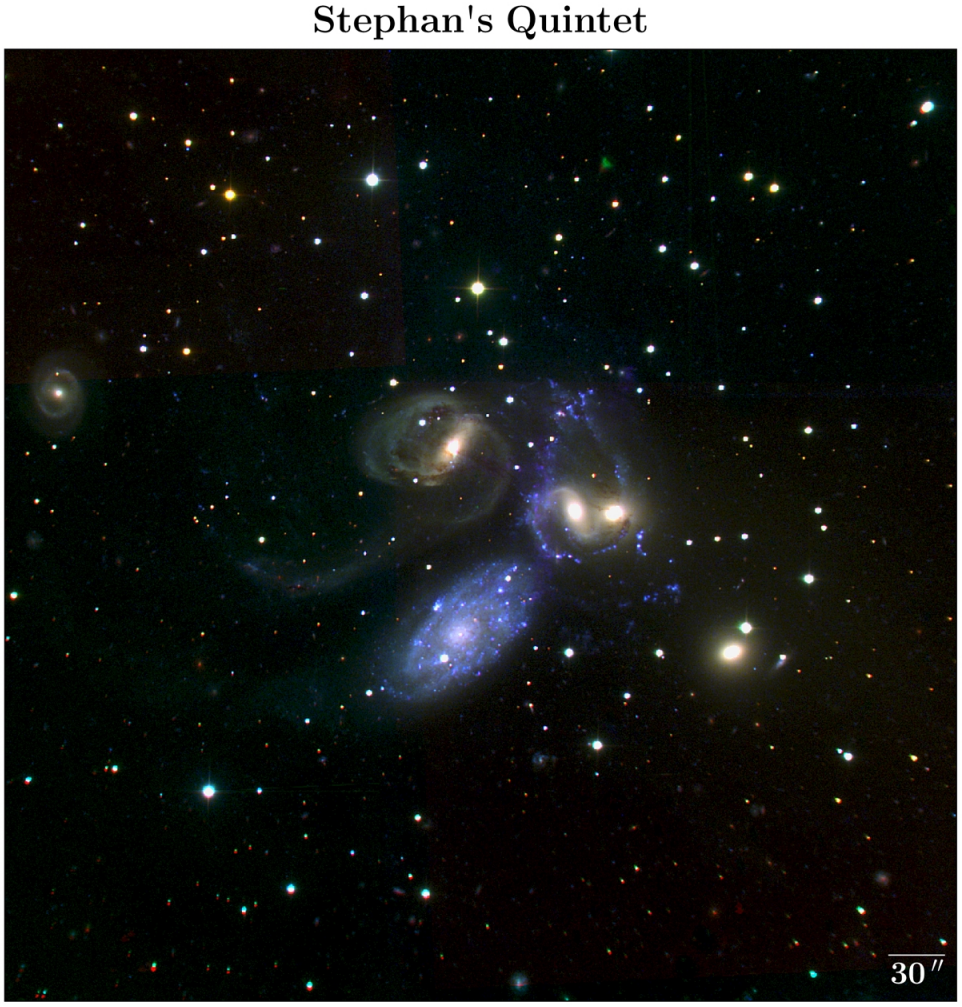

Paper I: 175 областей HII

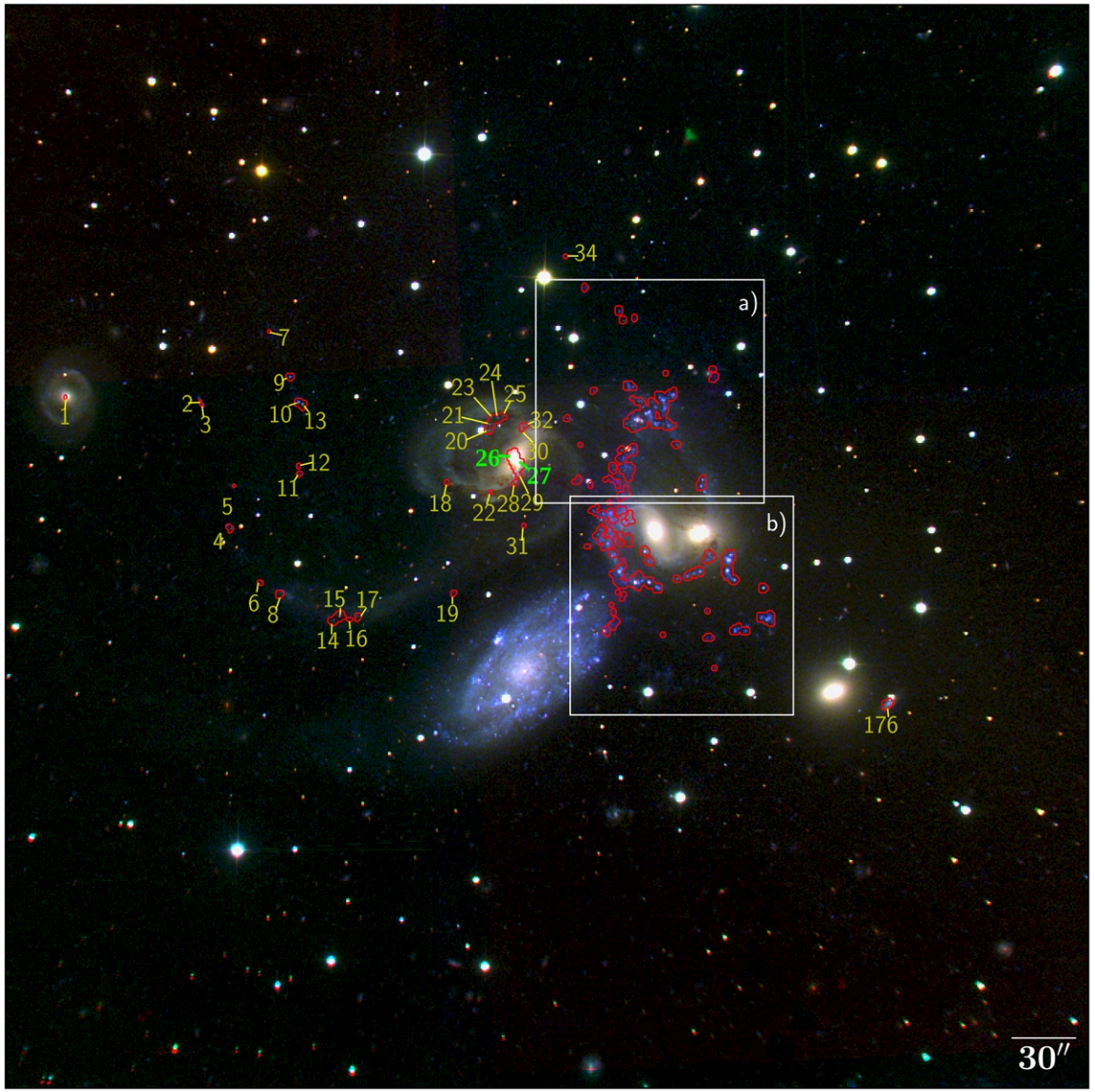

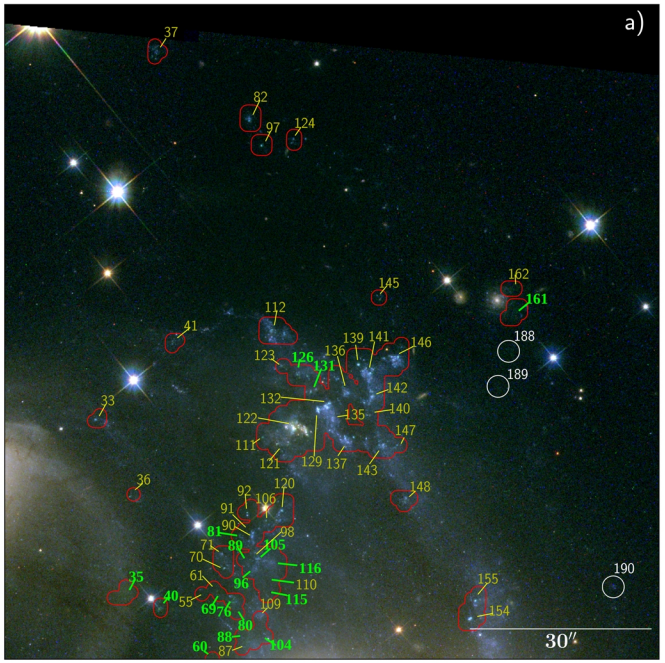

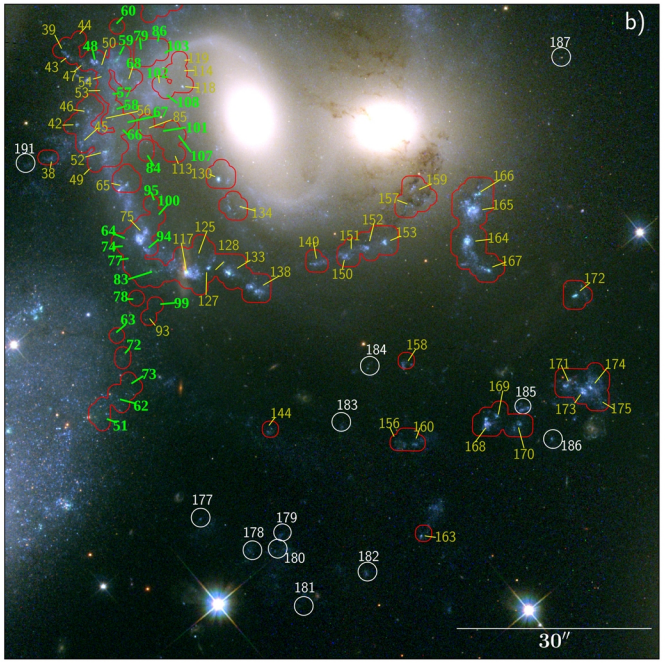

Paper I: по кинематике должен быть ударный фронт

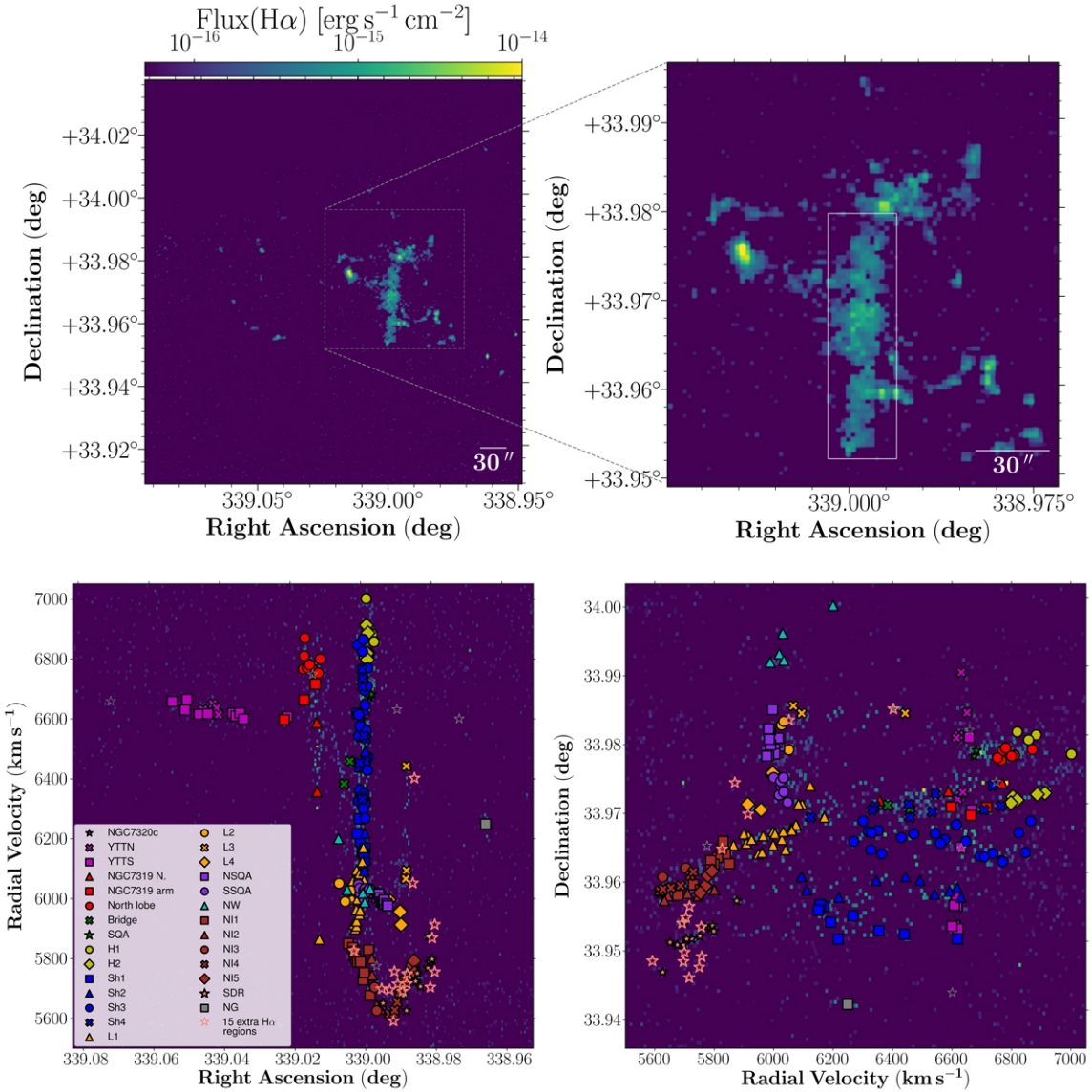

Present Paper II: диагностика по отношениям линий

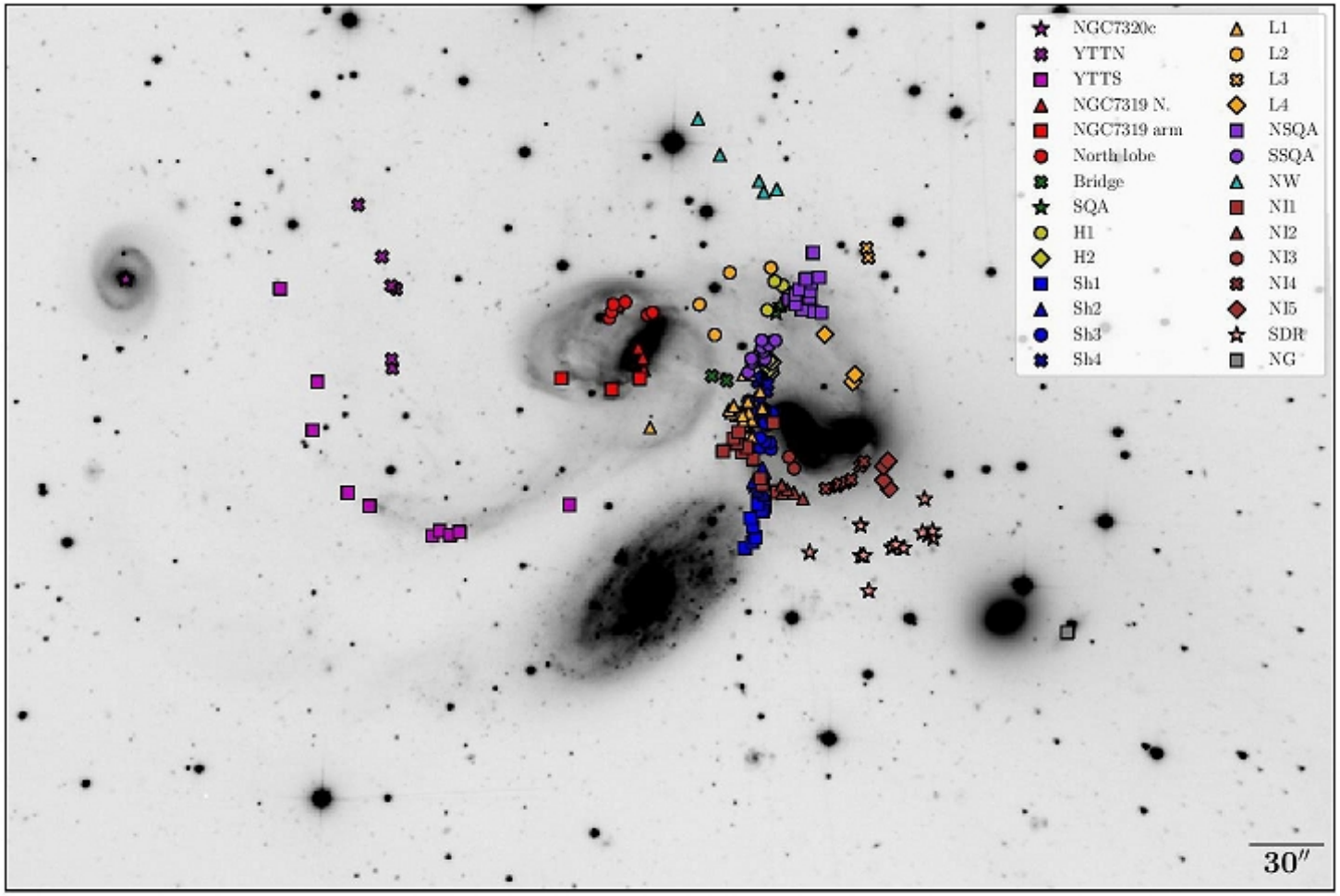

Fig. 3. Different systems of emission line objects defined here and indicated on SITELLE deep-greyscale image of SQ. The figure shows are the positions of YTTN and YTTS (magenta crosses and squares, respectively); NGC7319 nucleus, 'arm', and north lobe (red triangles, squares, and circles, respectively); bridge (green crosses); SQA (green stars); Hs (H1: yellow circles; H2: yellow diamonds); Shs (Sh1: blue squares; Sh2: blue triangles; Sh3: blue circles; Sh4: blue crosses); Ls (L1: orange triangles; L2: orange circles; L3: orange crosses; L4: orange diamonds); NSQA and SSQA (violet squares and circles); NW (cyan triangles); NIs (NI1: brown squares; NI2: brown triangles; NI3: brown circles; NI4: brown crosses; NI5: brown diamonds); SDR (salmon stars); and NG (grey squares).

Разделение по скоростям

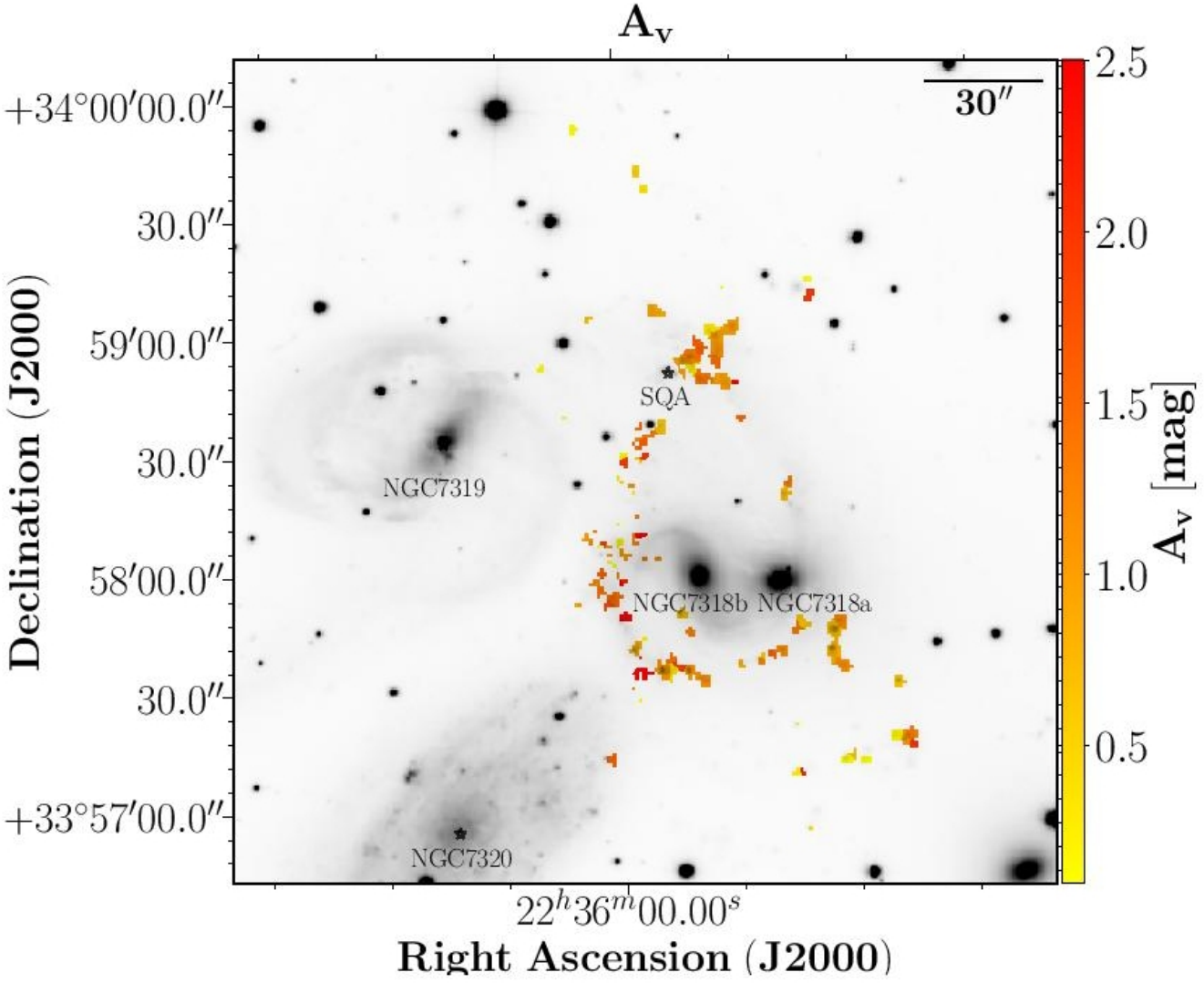

Отношения линий картируются

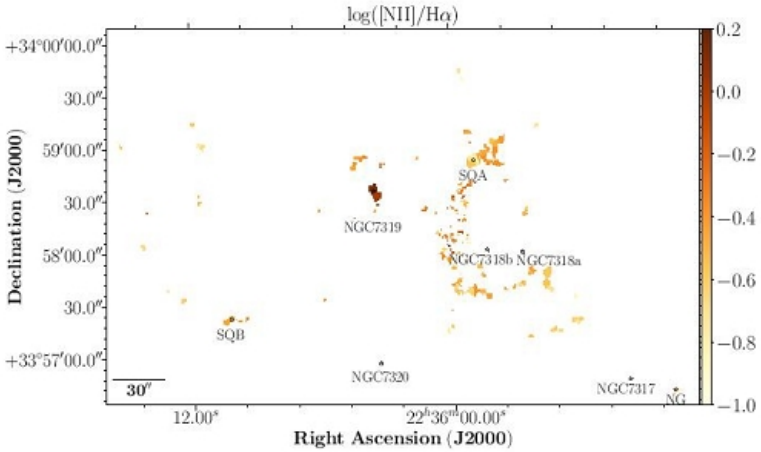

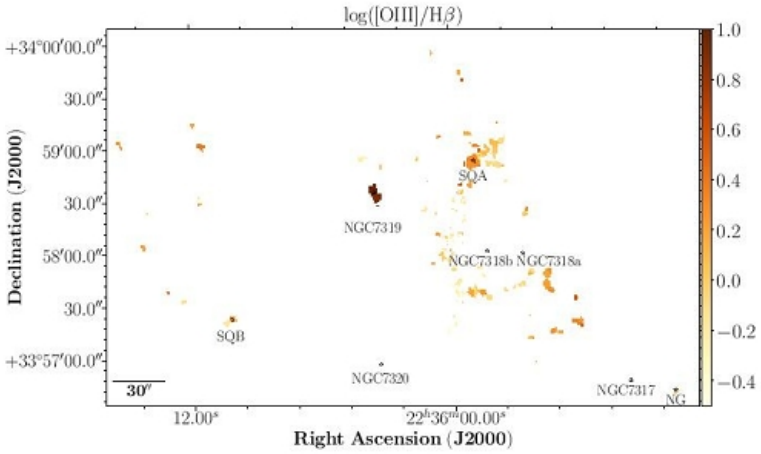

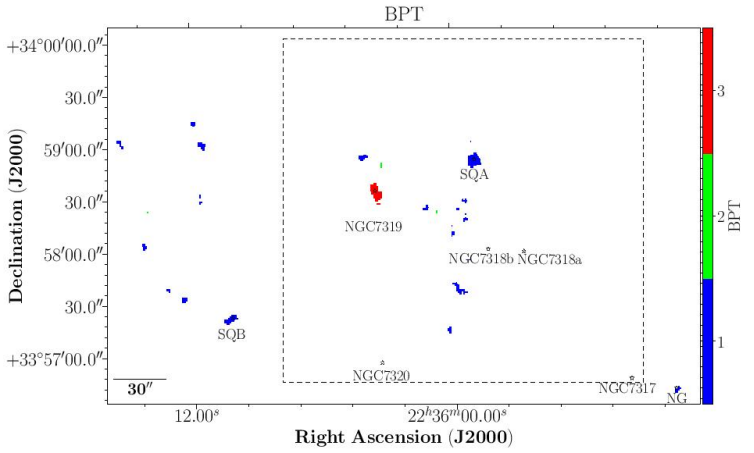

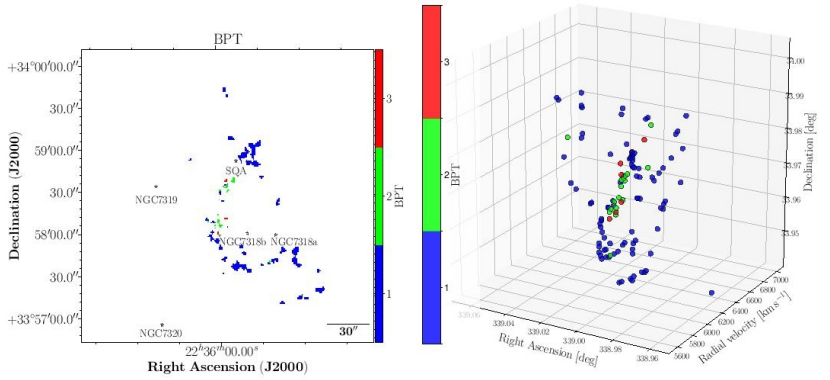

Fig. 8. Stephan's Quintet spatial map colour coded according to their position in the BPT diagnostic diagram for the HV sub-sample (upper panel), the LV sub-sample (lower left panel), and the three-dimensional distribution of the BPT class (α, δ, radial velocity; lower right panel). Blue, green, and red pixels represent star-forming (1), composite (2), and AGN-like (3) regions, respectively.

BPT-диагностика

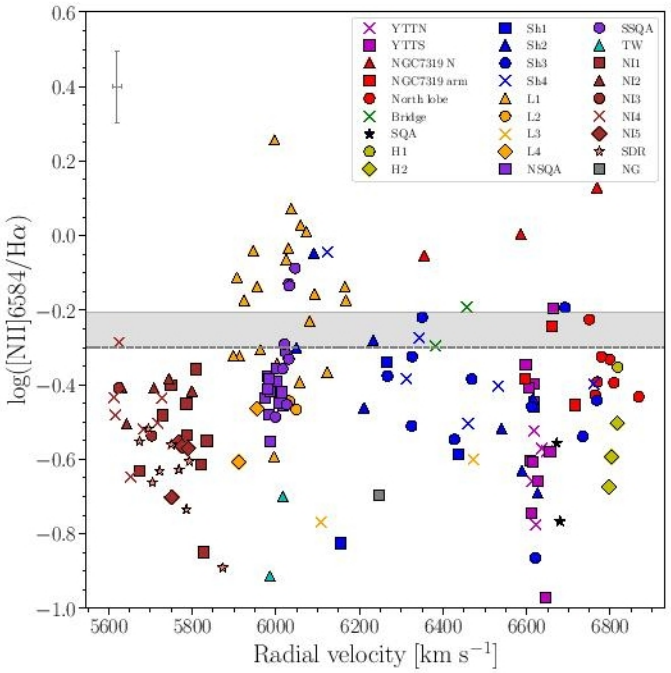

Fig. 4. Log([N II]/Hα) versus radial velocity diagram. All the points in the figure have the same colours and markers as Fig. 3. The horizontal dashed grey line and the grey band correspond to the reference value at log([N II]/Hα)=-0.3 and the uncertainties for the log([N II]/Hα) ratio, respectively. The upper left cross indicates the typical error of both parameters.

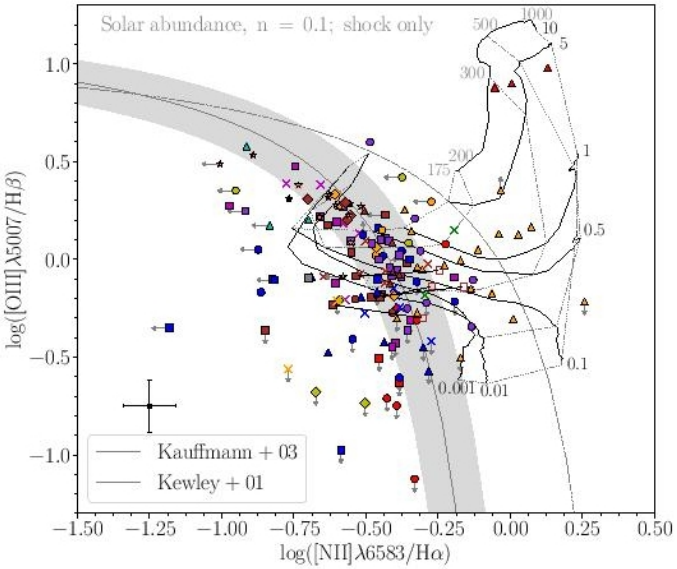

Fig. 7. Diagnostic diagram (BPT) of [O III]λ5007/Hβ versus [N II]λ6584/Hα for the SQ Hα emission regions. Regions without an arrow have a S/N higher than 3 for the fluxes in the strong emission lines Hα, Hβ, [O III]λ5007, and [N II]λ6584. The typical error in each axis is represent with a black cross. Regions with an ascending grey arrow have a S/N(Hβ)<3, regions with a decreasing grey arrow have a S/N([O III]λ5007)<3, while regions with a grey arrow pointing left have a S/N([N II]λ6584)<3. All the points in the figure have the same colours and markers as Fig. 3. The grey dashed line shows the Kewley et al. (2001) demarcation and the grey continuous line shows the Kauffmann et al. (2003) curve. The grey band shows the uncertainties for the BPT line ratios (i.e. [O III]λ5007/Hβ and [N II]λ6584/Hα) to the Kauffmann

Для HII-областей – темпы звездообразования и металличность

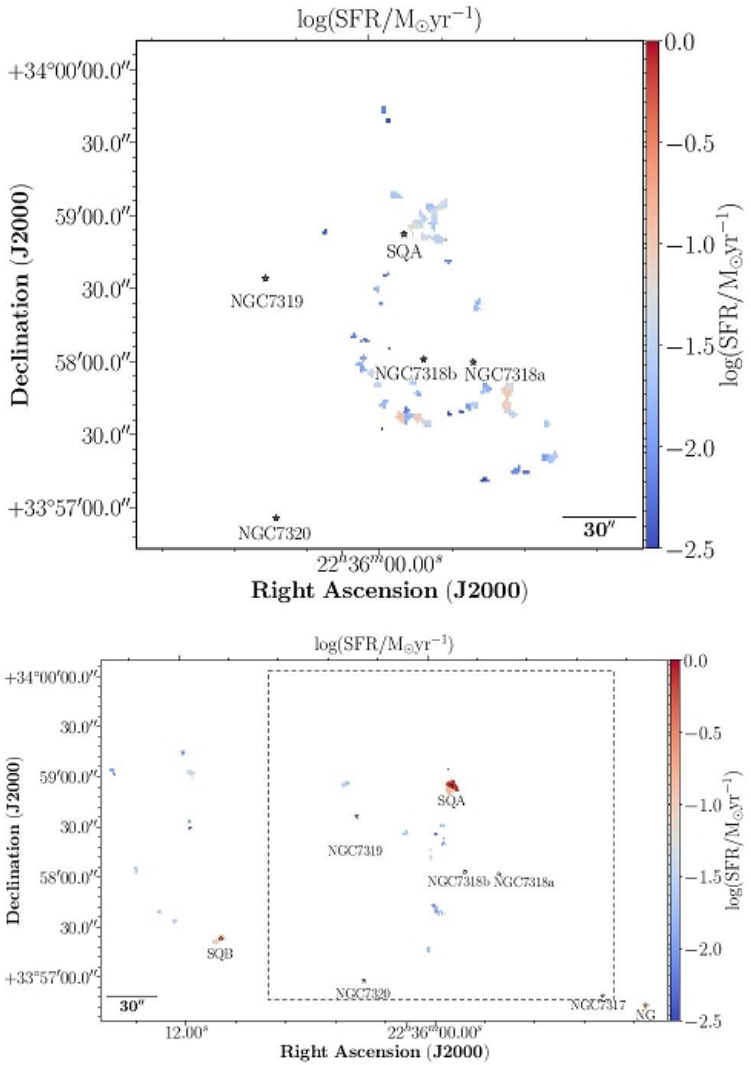

Fig. 10. Stephan's Quintet spatial map colour coded according to their SFR for the LV sub-sample (upper panel) and the HV sub-sample panel).

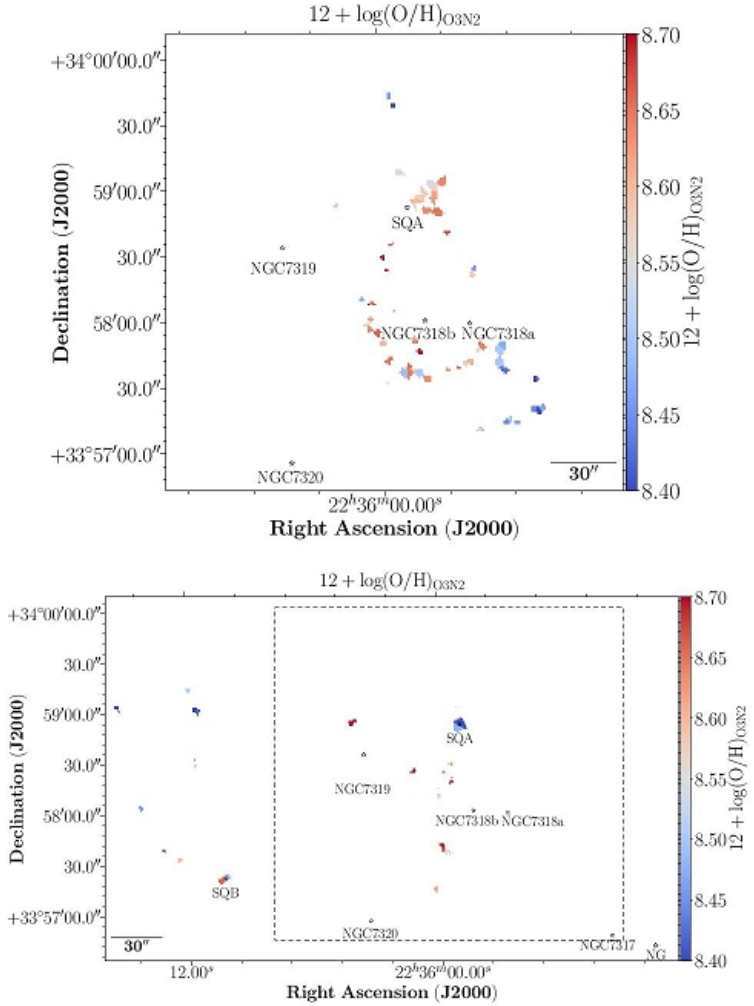

Fig. 11. Stephan's Quintet spatial map for the LV sub-sample (upper panel) and the HV sub-sample (lower panel) colour coded according to the 12+log(O/H) derived using the O3N2 calibrator from Pérez-Montero & Contini (2009).